

The logo for EPJ B consists of a dark blue rectangle with a red and orange abstract pattern on the left side. The text "EPJ B" is written in a white, serif font in the center of the blue area.

EPJ B

www.epj.org

Condensed Matter
and Complex Systems

Eur. Phys. J. B **68**, 487–494 (2009)

DOI: 10.1140/epjb/e2009-00111-x

Lateral shaping and stability of a stretching viscous sheet

B. Scheid, S. Quiligotti, B. Tran and H.A. Stone



Lateral shaping and stability of a stretching viscous sheet

B. Scheid^{1,a}, S. Quiligotti², B. Tran², and H.A. Stone¹

¹ School of Engineering and Applied Sciences, Harvard University, MA 02138 Cambridge, USA

² Saint-Gobain Recherche, 39 Quai Lucien Lefranc, B.P. 135, 93303 Aubervilliers Cedex, France

Received 24 July 2008 / Received in final form 13 January 2009

Published online 25 March 2009 – © EDP Sciences, Società Italiana di Fisica, Springer-Verlag 2009

Abstract. We investigate the changes of shape of a stretching viscous sheet by controlling the forcing at the lateral edges, which we refer to as lateral shaping. We propose a one-dimensional model to study the dynamics of the viscous sheet and systematically address stability with respect to draw resonance. Two classes of lateral forcing are considered: (i) for the case that the stress at the edges is specified, we show that a pure outward normal stress S_n is usually unfavorable to the draw resonance instability as compared to the case of stress-free lateral boundaries. Alternatively, a pure streamwise tangential stress S_t is stabilizing; (ii) for the case that the lateral velocity at the edges is specified, we show that the stability properties are problem specific but can be rationalized based on the induced stress components (S_n, S_t) .

PACS. 47.15.gm Thin film flows – 47.20.Gv Viscous and viscoelastic instabilities – 47.85.M- Material processing flows; industrial applications

1 Introduction

Stretching viscous sheets are frequently encountered in the polymer and glass manufacturing industries. During the pure longitudinal stretching of a thin sheet, the *width* usually shrinks from the inlet to the take-up due to the strong extensional deformation effected by the pulling. This necking phenomenon makes the sheet thickness thicker than expected from a pure parallel stretching. To prevent this response, it is common in processes such as polymer film casting to keep the distance between the inlet and the take-up roll as short as possible, so that the aspect ratio between the width and the length is usually of order of unity in such processes. In other processes such as the float-glass process, the aspect ratio of the viscous sheet can be much smaller than unity and mechanical stretching transverse to the main flow can be used to work against the neck-in effect, and thus obtain thinner sheets.

A mechanical system of lateral stretching was proposed by Pilkington [1] for the float-glass process and consists in edge rollers that grip the edges of a glass sheet and define its speed. In practice, the rollers are placed closer to the inlet than to the take-up. Therefore the glass sheet still shrinks in width between the last edge roll and the take-up. Narayanaswamy [2] proposed a one-dimensional model that describes this shrinking portion of a viscous sheet in the simplest possible terms, i.e. neglecting surface tension, inertia and hydrostatic pressure. In this region, it was assumed that there was no stress in the transverse direction,

which is valid only for small aspect ratios¹. The width and thickness of the glass sheet were then found to be attenuated in the same proportion, and satisfactory agreement with measured widths were obtained in the region past the last edge roller.

Silagy et al. [4] extended the one-dimensional model in [2] to sheets of larger aspect ratios by considering the edges of the sheet to be free surfaces. Consequently, the stress in the transverse direction depends instead on the edge curvature. Silagy et al. [5] further determined the threshold for the draw resonance instability of such stretching sheets with stress-free boundary conditions at the edges. The draw resonance instability is characterized by a periodic variation in the sheet's thickness around the centerline (see e.g. [3]), whose physical mechanism has been recently proposed in the case of heat transfer [6]. These thickness variations take place across the entire width, which also oscillates synchronously around the symmetry axis. It was found in [5] that the neck-in effect always has a stabilizing effect with respect to draw resonance, at least for aspect ratios of order unity. In this paper, we extend the one-dimensional model in [5] to lateral shaping, by which we refer to stress distributions (or speed) imposed along the edges.

In Section 2, we present the mathematical formulation of the 2D model, which is the basis from which we

¹ A way to appreciate this assumption is to consider the limit where the width is as small as the thickness (aspect ratio $\ll 1$), which corresponds to the slender (or fiber) limit for which the stress in the transverse (or radial) direction is negligible compared to the axial stress (see e.g. [3]).

^a e-mail: bscheid@seas.harvard.edu

construct a 1D model. In Section 3 we discuss the case of a stress specified at the edges and explore the different limiting cases. In Section 4 we alternatively consider the case of a transverse speed specified at the edges. In each case, the stability of solutions is investigated systematically. Concluding remarks are given in Section 5.

2 Mathematical formulation

2.1 Two-dimensional equations

We consider a three-dimensional viscous liquid sheet with thickness h_0 , velocity u_0 and width $2\ell_0$ at the inlet being stretched over a length L to the take-up speed u_L , as sketched in Figure 1. The draw ratio is denoted $Dr = u_L/u_0$. The sheet is also shaped in the lateral direction by a symmetrically applied stress $\mathbf{S} = S_n \mathbf{n} + S_t \mathbf{t}$ (only represented on one edge in Fig. 1). The coordinate system is chosen with x axial and z transverse in the width direction. The position of the lateral boundary is defined as $z = \ell(x, t)$. Variables are made dimensionless through the transformations: $h \rightarrow h_0 h$, $x \rightarrow Lx$, $\ell \rightarrow \ell_0 \ell$, $z \rightarrow \ell_0 z$, $u \rightarrow u_0 u$, $w \rightarrow u_0 w$ and $t \rightarrow (L/u_0)t$. The stress is scaled by $\mu u_0/L$ with μ the dynamic viscosity of the fluid.

We define the *film parameter* $\varepsilon = h_0/L$ and the *aspect ratio* $a = \ell_0/L$. Neglecting inertia, gravity and surface tension, and using the standard thin-film assumption $\varepsilon \ll 1$, the continuity and Stokes equations, as shown by Yeow [7], reduce to a two-dimensional system of evolution equations for the sheet thickness $h = h(x, z, t)$ and in-plane velocities $u = u(x, z, t)$ and $w = w(x, z, t)$,

$$\partial_t h + \partial_x(uh) + \frac{1}{a} \partial_z(wh) = 0, \quad (1a)$$

$$\partial_x(h\sigma_{xx}) + \frac{1}{a} \partial_z(h\sigma_{xz}) = 0, \quad (1b)$$

$$\partial_x(h\sigma_{xz}) + \frac{1}{a} \partial_z(h\sigma_{zz}) = 0, \quad (1c)$$

with the components of the in-plane stress tensor,

$$\sigma_{xx} = 4\partial_x u + \frac{2}{a} \partial_z w, \quad (2a)$$

$$\sigma_{zz} = \frac{4}{a} \partial_z w + 2\partial_x u, \quad (2b)$$

$$\sigma_{xz} = \frac{1}{a} \partial_z u + \partial_x w. \quad (2c)$$

The boundary conditions in the axial direction are

$$\ell(0, t) = h(0, z, t) = u(0, z, t) = 1, \quad (3a)$$

$$u(1, z, t) = Dr, \quad (3b)$$

and the the boundary conditions in the transverse direction are, at $z = 0$, the symmetry conditions,

$$w|_0 = \sigma_{xz}|_0 = 0, \quad (4)$$

and at the edge $z = \ell(x, t)$ the kinematic condition and the stress balance, respectively,

$$a(\partial_t \ell + u|_\ell \partial_x \ell) = w|_\ell, \quad (5a)$$

$$\mathbf{n} \cdot \boldsymbol{\sigma}|_\ell = \mathbf{S}. \quad (5b)$$

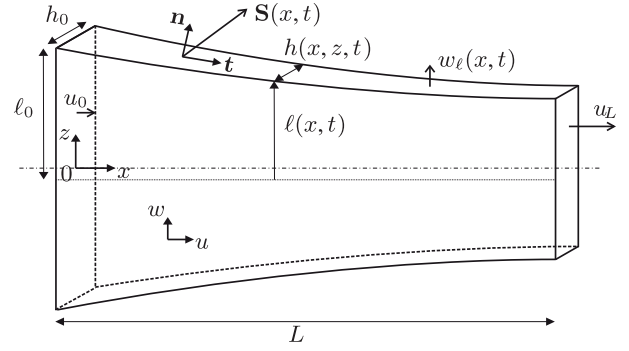


Fig. 1. Stretching viscous sheet with stress \mathbf{S} and transverse speed w_ℓ at the boundary $z = \ell(x, t)$.

The normal and tangential unit vectors are, respectively, $\mathbf{n} = (-a\partial_x \ell, 1)/n$ and $\mathbf{t} = (1, a\partial_x \ell)/n$, with $n = (1 + (a\partial_x \ell)^2)^{1/2}$. The normal and tangential projections of the stress balance (5b) are thus

$$\sigma_{zz}|_\ell - 2a\partial_x \ell \sigma_{xz}|_\ell + (a\partial_x \ell)^2 \sigma_{xx}|_\ell = n^2 S_n, \quad (6a)$$

$$a\partial_x \ell (\sigma_{zz}|_\ell - \sigma_{xx}|_\ell) + (1 - (a\partial_x \ell)^2) \sigma_{xz}|_\ell = n^2 S_t. \quad (6b)$$

The two-dimensional model (1–5b) has been solved numerically by several authors with the stress-free boundary condition $\mathbf{S} = \mathbf{0}$ (see e.g. [8] and references therein). We have performed 2D numerical computations with $\mathbf{S} \neq \mathbf{0}$ in order to validate some of the results obtained with the one-dimensional model developed in the next section. For the 2D numerical simulations, we have used COMSOL software. Due to the large deformations which the fluid undergoes in the present lateral stretching problem, a purely Lagrangian reference frame where the mesh follows the fluid particles is not practical. Instead the software COMSOL allows to use an intermediate between the traditional Eulerian reference frame and the Lagrangian reference frame. This hybrid is commonly known as the Arbitrary Lagrangian-Eulerian (ALE) reference frame [9]. The basic idea is to allow the mesh to deform arbitrarily (but preferably smoothly) in the bulk but still keep track of the interface of the liquid.

2.2 Constructing the 1D model

With the goal of obtaining a one-dimensional model, we integrate the continuity equation (1a) and the streamwise momentum equation (1b) along half the width and use the boundary conditions (4) and (5a) to obtain

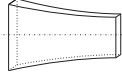

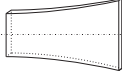
$$\partial_t \int_0^\ell h dz + \partial_x \int_0^\ell uh dz = 0, \quad (7)$$

$$\partial_x \int_0^\ell h\sigma_{xx} dz - h|_\ell \sigma_{xx}|_\ell \partial_x \ell + \frac{1}{a} h|_\ell \sigma_{xz}|_\ell = 0. \quad (8)$$

We next assume $|a\partial_x \ell| \ll 1$ and truncate (6b) after $O(a\partial_x \ell)^2$ to obtain

$$\sigma_{xz}|_\ell = a\partial_x \ell (\sigma_{xx}|_\ell - \sigma_{zz}|_\ell) + (1 + 2(a\partial_x \ell)^2) S_t, \quad (9)$$

Table 1. Typical shapes of two-dimensional stretching sheets versus various boundary conditions (see text for details). $S_n^*(x, t)$ is the normal stress that keeps the width constant.

Edge boundary conditions				Section
Stress-free: $S_n = 0, S_t = 0$	$a \rightarrow \varepsilon$ 1D fiber [10]	finite a 2D sheet [4]	$a \rightarrow \infty$ 1D sheet [7]	not possible 3.1
Pure normal stress: $S_n = S_n(x, t)$	$S_n < S_n^*$	$S_n = S_n^*$	$S_n > S_n^*$	3.2
Pure tangential stress: $S_t = c^{\text{ste}}$	$S_t < 0$ or $S_t > 0$	not possible		3.3
Specified velocity: $w_\ell = w_\ell(x)$	$w_\ell < 0$	$w_\ell = 0$	$w_\ell > 0$	4

which substituted in (6a), and also truncated after $O(a\partial_x\ell)^2$, leads to

$$\sigma_{zz}|_\ell = (a\partial_x\ell)^2\sigma_{xx}|_\ell + (1 - (a\partial_x\ell)^2)S_n + 2(a\partial_x\ell)S_t. \quad (10)$$

Based on previous studies of 2D sheets [2,4], we pose the ansatz

$$u = u(x, t), \quad h = h(x, t) \quad \text{and} \quad w = \frac{w_\ell(x, t)}{\ell(x, t)}z, \quad (11)$$

which assumes the axial velocity u and the thickness h to be one-dimensional, and the transverse velocity w to vary linearly with the z -coordinate, with $w_\ell(x, t) = w|_\ell$ denoting the transverse velocity at the edge boundary. With this ansatz, the continuity equation (7) and the kinematic condition (5a) become

$$\partial_t(\ell h) + \partial_x(\ell h u) = 0, \quad (12a)$$

$$\partial_t\ell + u\partial_x\ell - \frac{w_\ell}{a} = 0, \quad (12b)$$

and the stress components (2) take the forms

$$\sigma_{xx} = 4\partial_x u + \frac{2w_\ell}{a\ell}, \quad (13a)$$

$$\sigma_{zz} = 2\partial_x u + \frac{4w_\ell}{a\ell}, \quad (13b)$$

$$\sigma_{xz} = z\partial_x\left(\frac{w_\ell}{\ell}\right). \quad (13c)$$

We notice that σ_{xx} and σ_{zz} are now z -independent, which makes the normal stress boundary condition (10) true everywhere in the domain and not only at the boundary ($z = \ell$). The form of the stress balance (8) will depend on whether we specify the stress components (S_n, S_t) or the transverse velocity (w_ℓ) at the edge, as investigated in Sections 3 and 4, respectively. To specify S_n and S_t , we will use (9, 10) and truncate (8) after $O(a\partial_x\ell)^2$ to write

$$a\partial_x(h\ell\sigma_{xx}) = h(S_n a\partial_x\ell - S_t), \quad (14)$$

while to specify w_ℓ , we will use (13c) in (8) and write

$$a\partial_x(h\sigma_{xx}) = -h\partial_x\left(\frac{w_\ell}{\ell}\right). \quad (15)$$

The different situations investigated in this paper are classified in Table 1 relative to the boundary conditions and the expected shapes of a two-dimensional stretching sheet. The last column refers to the corresponding sections of the paper.

2.3 Linear stability analysis

Depending on the lateral boundary condition to be considered (as classified in Tab. 1), the system of PDEs to be solved will differ as described in the subsequent sections. Nevertheless, the way the linear stability analysis is performed remains generic and is outlined in this section. The analysis consists in solving for the unknowns h, ℓ, u and σ_{xx} , which can be rewritten in a perturbative form as

$$h(x, t) = h_s(x) (1 + H(x) e^{\lambda t}), \quad (16a)$$

$$\ell(x, t) = \ell_s(x) (1 + L(x) e^{\lambda t}), \quad (16b)$$

$$u(x, t) = u_s(x) (1 + U(x) e^{\lambda t}), \quad (16c)$$

$$\sigma_{xx}(x, t) = \sigma_{xx_s}(x) (1 + \Sigma(x) e^{\lambda t}), \quad (16d)$$

where h_s, u_s, ℓ_s and σ_{xx_s} are the real steady-state solutions, H, L, U and Σ are the complex perturbations, and $\lambda = \lambda_R + i\lambda_I$ is the complex eigenvalue with λ_R the growth rate and λ_I the frequency. The steady-state solutions and the linearized perturbations will be sought together using the following axial boundary conditions

$$h_s(0) = \ell_s(0) = u_s(0) = 1, \quad \sigma_{xx_s}(0) = f_{s_0}, \quad (17a)$$

$$H(0) = L(0) = U(0) = U(1) = 0, \quad \Sigma(0) = F_0, \quad (17b)$$

where f_{s_0} is the axial tension at the inlet ($x = 0$) and F_0 is the corresponding perturbation. Both f_{s_0} and F_0 are real parameters that are prescribed a priori. Therefore at any given value of f_{s_0} corresponds a steady state from which the draw ratio can be deduced, namely $Dr = u_s(1)$. Furthermore, the magnitude of F_0 sets the relative amplitudes of the linearized perturbations for the stability analysis; its value has been fixed for all calculations to $F_0 = 0.1$.

Solutions to the problem corresponding to a specific lateral condition (see Tab. 1) will next be computed by continuation using the ODE solver AUTO-07P [11]. Having four real unknowns ($h_s, u_s, \ell_s, \sigma_{xx_s}$) with four real boundary conditions (17a) and four complex unknowns (H, U, L, Σ) with five complex boundary conditions (17b), the continuation requires three free parameters (see [12] for details), namely f_{s_0}, λ_R and λ_I . The basic idea behind the continuation method is to suppose that one knows a solution of the problem at hand and that this solution is not isolated in the parameter space but lies on a continuous branch of solutions. Then, the software AUTO-07P

proceeds to construct the whole branch of solutions in small steps, using the Newton iteration method, starting from the known solution. Here however for a particular f_{s_0} (or equivalently Dr), the number of eigenvalues λ for which the eigenvalue problem has non-trivial solutions is denumerably infinite – see e.g. the work by Yeow [7] who has computed the first three eigenvalues. Having thus an infinite number of modes, we will choose the branch of solutions for the first mode (or eigenvalue) corresponding to the most dangerous one and additionally restrict the analysis to the neutral stability curve obtained for a zero growth rate $\lambda_R = 0$. The corresponding solutions in the 1D case (e.g. either for $a \rightarrow 0$ or $a \rightarrow \infty$ as shown below) have analytical expressions – for the steady-state solutions and the linearized perturbations – that can be found in the work by Renardy [13] and have thus been used here as starting solutions.

Finally, having fixed λ_R , and provided the number of boundary conditions (17), one needs an additional free parameter in order to construct the neutral curve, i.e. the branch of solutions at the instability threshold. This free parameter can either be the aspect ratio a (starting from the known solution at $a = 0$) for the stress-free lateral boundary condition (see Sect. 3.1), or, for a fixed value of a , another parameter that probes a specific lateral boundary condition like the normal stress parameter b (see Sect. 3.2), the tangential stress parameter S_t (Sect. 3.3) and the amplitude B of the transverse velocity function (Sect. 4). These different cases are treated individually in the remaining sections of the paper.

2.4 Axial tension

In order to have more insights into the physical mechanisms involved in 2D stretching and possible instabilities, we want to evaluate the axial force or tension, denoted $f(x, t)$, in the sheet. As in the previous section, we present here what is generic and will examine in the following section what is specific for each lateral boundary condition.

For steady-state conditions, the continuity and kinematic equations (12) become

$$(\ell_s h_s u_s)' = 0, \quad (18a)$$

$$\ell_s' = \frac{w \ell_s}{a u_s}, \quad (18b)$$

where a prime denotes the x -derivative. Using the boundary conditions (17a) and (18a) yields

$$h_s \ell_s u_s = 1. \quad (18c)$$

Now combining the steady-state results (18) with (13a) yields

$$\frac{h_s'}{h_s} + \frac{\ell_s'}{2\ell_s} = -\frac{h_s \ell_s \sigma_{xxs}}{4} \equiv -\frac{f_s(x)}{4}, \quad (19)$$

where f_s is the steady-state tension. Equation (19) thus relates the shape variation of the sheet to the axial tension, whose distribution along x direction will depend on the lateral boundary conditions.

3 Specified lateral stress

In the case we want to prescribe the stress applied at the edges of the sheet, we can recast the stress relations (13a) and (13b) as

$$\sigma_{xx} = 2\sigma_{zz} - 6\frac{w_\ell}{a\ell}, \quad (20a)$$

$$\sigma_{zz} = 2\sigma_{xx} - 6\partial_x u, \quad (20b)$$

and then rewrite them using (10) in order to eliminate σ_{zz} ,

$$(1 - 2(a\partial_x \ell)^2) \sigma_{xx} + 6\frac{w_\ell}{a\ell} = 2(1 - (a\partial_x \ell)^2) S_n + 4a\partial_x \ell S_t, \quad (21a)$$

$$(2 - (a\partial_x \ell)^2) \sigma_{xx} - 6\partial_x u = (1 - (a\partial_x \ell)^2) S_n + 2a\partial_x \ell S_t. \quad (21b)$$

Let us now consider the different cases and limits as classified in Table 1. Note the model proposed here extends to non-zero lateral stresses (i.e. $S_n \neq 0$ and/or $S_t \neq 0$) the model proposed by Silagy et al. [4] for stress-free condition ($S_n = S_t = 0$).

3.1 Stress free (short review): $S_n = S_t = 0$

For stress-free conditions, we can integrate (14) once to obtain

$$h\ell\sigma_{xx} = f(t), \quad (22)$$

where $f(t)$ is the axial tension, which is now independent of x . For steady-state conditions, and using (18), (22) then becomes

$$h_s \ell_s \sigma_{xxs} = f_s = \text{constant} \quad (23)$$

with $f_s = f_{s_0}$ based on (17a). Consequently, replacing (23) in (19) shows that a decrease of the width due to the necking phenomenon is automatically accompanied by an increase of the thickness, as was mentioned in the Introduction.

The system of equations used for the linear stability analysis, setting $S_n = S_t = 0$ as done in [4], is obtained by eliminating first w_ℓ in (12b) from (21a), and by substituting then (16) into (12a), (12b), (21b) and (22). We then followed the steps for the instability analysis given in Section 2.3. Results are shown in Figure 2 for the stability threshold of the draw resonance, as measured by the critical draw ratio Dr_c for the entire range of aspect ratios a . We notice that Silagy et al. [4,5] have only plotted the right part of the neutral curve for $0.5 < a < \infty$ and have not extended the curve for $a \rightarrow 0$. They have also compared the neutral curve obtained with the 1D model to the one computed from 2D time-dependent simulations and have found a good qualitative agreement, although the peak in the neutral curve is shifted to $a \approx 1$ and $Dr_c \approx 40$. Nevertheless, away from the peak, the error is smaller and should even vanish when approaching the 1D limits.

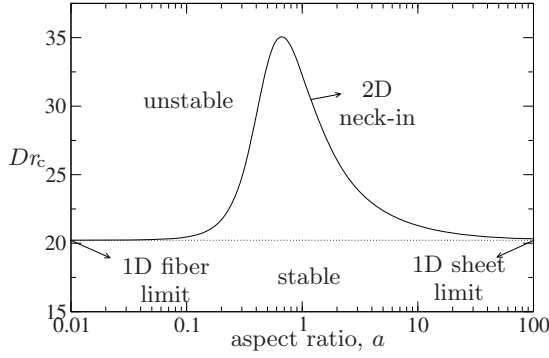


Fig. 2. Stability map for the draw resonance of a stretching 2D sheet with stress-free conditions $S_n = S_t = 0$ (solid line). The 1D limit corresponds to $Dr_c = 20.218$ (dotted line).

Figure 2 shows essentially that the 2D neck-in effect is always stabilizing as compared to a pure 1D stretching, i.e. $Dr_c^{(2D)} > Dr_c^{(1D)} = 20.218$ (see also [5]). This stabilization is maximum for $a = O(1)$ and disappears on both sides corresponding to the following limits:

- **Fiber limit** ($a \rightarrow \varepsilon$): pure 1D stretching can be recovered in the limit of small aspect ratios, namely $a \rightarrow \varepsilon$, which means the width and the thickness are of the same order of magnitude. Neglecting the $O(a^2)$ -terms in (21b), with $S_n = S_t = 0$, gives

$$\sigma_{xx} = 3\partial_x u, \quad (24)$$

which is the stress relation for fiber spinning [10], where 3 is the Trouton ratio. The system of equations is then solved for both the extensional velocity u and the fiber cross-sectional area $\propto \ell h$, after substituting (24) in (12a) and (22). In this limit, note from (13b) that the transverse stress is $\sigma_{zz} = 0$, as was mentioned in the Introduction.

- **Constant-width 1D sheet limit** ($a \rightarrow \infty$): the other limit that leads to a pure 1D stretching is the case of an infinitely wide sheet, i.e. $a \rightarrow \infty$. Therefore from (12b), the width remains constant, $\ell = 1$, such that the edges have no lateral motion, i.e. $w_\ell = 0$. Consequently, the stress relation (13a) is

$$\sigma_{xx} = 4\partial_x u, \quad (25)$$

as first shown by Taylor [14]. Yeow [7] demonstrated in turn that the model for fiber spinning and constant-width film casting are mathematically identical. Consequently, the critical draw ratio for draw resonance is identical for both, i.e. $Dr_c^{(1D)} = 20.218$. Indeed the Trouton ratio can be scaled out together with the viscosity. It is common to speak about “effective” or “extensional” viscosity that is therefore 3μ for fibers and 4μ for sheets.

In contrast to the fiber limit, a sheet of constant width has a non-zero transverse stress equal to the half of the axial stress,

$$\sigma_{zz}|_{\ell=1} = 2\partial_x u, \quad (26)$$

as found from (13b) with $w_\ell = 0$.

3.2 Pure normal stress: $S_n \neq 0$ and $S_t = 0$

As indicated above, a sheet of finite aspect ratio experiences the neck-in effect but can be forced to have a constant width by applying a stress $S_n^*(x, t) = 2\partial_x u$ at the edge (see (26)). This lateral stress must be specified in order to produce a parallel flow and counterbalance lateral stresses concomitant to the neck-in effect of a two-dimensional stretching sheet. Assuming it is feasible in practice to control the normal stress both in space and in time all along the edges of the sheet, we can investigate the departure from the different reference cases outlined in Section 3.1. Let us thus specify

$$S_n(x, t) = bS_n^* = 2b\partial_x u \quad \text{and} \quad S_t = 0, \quad (27)$$

where b is a normal stress parameter. The constant-width case corresponds to $b = 1$ and the stress-free case is in turn recovered for $b = 0$. Incorporating (27) into (14) gives

$$\partial_x \sigma_{xx} = -\sigma_{xx} \frac{\partial_x(h\ell)}{h\ell} + 2b\partial_x u \frac{\partial_x \ell}{\ell}, \quad (28)$$

and upon substituting into (21b), while neglecting terms of $O(a\partial_x \ell)^4$, we find

$$\partial_x u = \frac{\sigma_{xx}}{(3+b)} \left(1 - (a\partial_x \ell)^2 \frac{(3-b)}{2(3+b)} \right). \quad (29)$$

Eliminating w_ℓ in (12b), using (13a), we also obtain

$$\partial_t \ell + u\partial_x \ell = \frac{\ell}{2} (\sigma_{xx} - 4\partial_x u). \quad (30)$$

The system of equations (28–30) and (12a), for the unknowns h , ℓ , u and σ_{xx} , is used to perform the linear stability analysis as described in Section 2.3. Notice the normal stress S_n at the boundary is also perturbed here, since $S_n^* = 2\partial_x u$. This point is discussed at the end of the section. Also, explicit ODE for u_s and ℓ_s are obtained by solving equations (29–30) for u'_s and ℓ'_s , and taking the roots corresponding to $u'_s > 0$ since $Dr > 1$.

We are now able to address the stability of laterally stretched sheets ($b \neq 0$). In Figure 3, results for $b < 1$, i.e. the width is everywhere narrower than the inlet width ($\ell_s \leq 1$), show that the system in this case is always more stable than with constant width ($b = 1$). Moreover, a sheet is also more stable than with stress-free edges ($b = 0$) for small aspect ratios but less stable for larger aspect ratios (e.g. the transition is at $a \approx 0.3$ for $b = 0.5$). Unfortunately, we were unable to find a physical mechanism for this non-monotonic behavior. Now results for $b > 1$, i.e. the width is everywhere wider than the inlet width, show that the system in this case is always less stable than with both constant-width and stress-free edges². Computations terminate where the basic assumption $a|\partial_x \ell| \ll 1$ is violated; we fixed the limit of applicability at $a|\partial_x \ell| \approx 0.5$ for the results plotted in Figure 3 and Figure 4a below.

It is also informative to show in Figure 4a a cross-plot of Figure 3 in which the stability limits are function of

² As pointed out by a referee, for $b > 1$, $Dr_c \approx Dr_c^{(1D)}/b$.

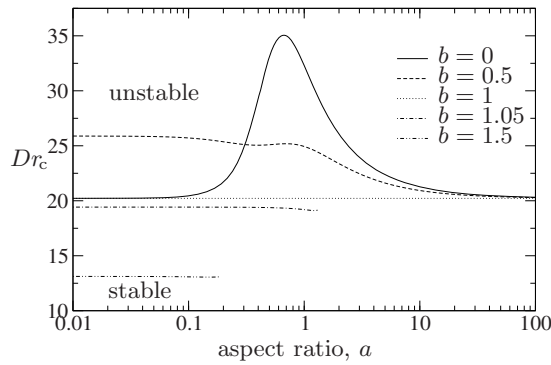


Fig. 3. Neutral stability curves as in Figure 2 for various values of the normal stress parameter b .

the normal stress parameter b for various aspect ratios. Figure 4b shows corresponding steady-state solutions for $a = 1/10$ (solid line in Fig. 4a) and various values of the parameter b . For small enough aspect ratios, $a \leq 1/4$, Figure 4a shows that pulling apart the edges of the sheet by increasing b from zero is first stabilizing and then destabilizing as b approaches unity. In contrast, for $a = 1/2$, the stabilization is maximum for $b = 0$ and increasing b has only a destabilizing effect. In either case, the critical draw ratio is always larger than 20.218 for $b < 1$, as was shown in Figure 3.

The steady-state axial tension in the sheet can be computed from (29). By neglecting the terms of $O(a\ell_s')^2$ for the sake of simplicity, and using (18a), we obtain

$$f_s = h_s \ell_s \sigma_{xxs} = -(3+b) \frac{(h_s \ell_s)'}{h_s \ell_s}. \quad (31)$$

The tension is thus related to the normalized axial variation of the cross-sectional area $h_s \ell_s$. Combining (31) and (19), yields

$$\frac{\ell_s'}{\ell_s} = \left(\frac{1-b}{1+b} \right) \frac{h_s'}{h_s}. \quad (32)$$

This result shows that in the limit of $a\ell_s' \ll 1$, the width and thickness of the sheet vary in the same proportion. The physical interpretation of the results shown in Figures 3 and 4 is thus that the residual neck-in effect when $b < 1$ causes the thickness at take-up to be larger than its value $1/20.218$ for a sheet of constant width, which is a response in favor of stability, as it was the case for the stress-free condition demonstrated in Section 3.1. The opposite is true for $b > 1$. These results indicate that conditions that lead to more *unstable* flow states can be generated when outward stress is applied perpendicular to the edge of the sheet.

Additionally, motivated by applications such as float glass that distribute rollers along the sheet, we look at a specified normal stress that is dependent on position but independent of time. Thus we take

$$S_n(x) = 2bu_s' \quad \text{and} \quad S_t = 0, \quad (33)$$

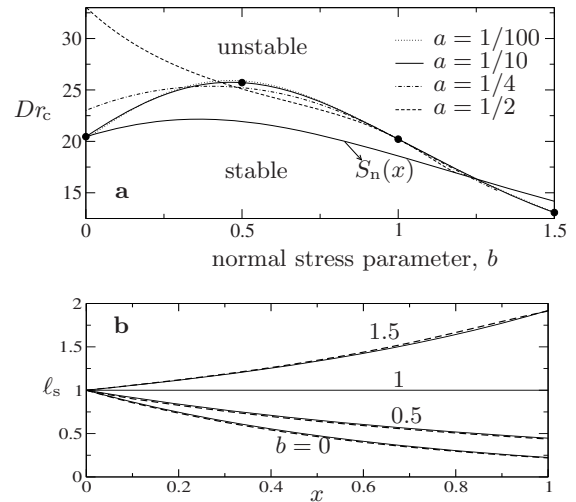


Fig. 4. (a) Neutral stability curves in function of the normal stress parameter b for various aspect ratios a and $S_t = 0$. (b) steady-state solutions for $a = 1/10$ (solid lines) and with 2D COMSOL solutions (dashed lines).

such that the specified normal stress depends only on the coordinate x through the steady-state velocity u_s . In contrast to (27), (33) is not perturbed in the stability analysis. The neutral stability curve is plotted for $a = 1/10$ in Figure 4a. Again, we find the lateral forcing to be stabilizing for $b < 1$ and destabilizing for $b > 1$ but with less intensity that when S_n was time-dependent, which suggests that control of the stability is possible by applying time-dependent lateral forcing. This result of lateral forcing should be of particular interest since no control appears to be efficient by applying purely axial forcing as was demonstrated by Renardy [13] in the 1D case.

3.3 Pure tangential stress: $S_n = 0$ and $S_t \neq 0$

We address here the effect of a pure tangential stress specified at the lateral edges and study how it affects the shape of the sheet and its stability, in the same manner we have investigated the effects of a pure normal stress in the previous section. For the sake of simplicity, we chose the tangential stress S_t to be constant. The set of equations to be solved for the linear stability analysis in this case, setting $S_n = 0$, are (14) rewritten as

$$\partial_x \sigma_{xx} = -\sigma_{xx} \left(\frac{\partial_x h}{h} + \frac{\partial_x \ell}{\ell} \right) - \frac{S_t}{a\ell}, \quad (34)$$

and (21b), neglecting terms of $O(a\partial_x \ell)^4$,

$$\partial_x u = \frac{\sigma_{xx}}{6} \left(2 - (a\partial_x \ell)^2 \right) - \frac{a}{3} S_t \partial_x \ell. \quad (35)$$

The above equations are completed with (12a) and (30).

Figure 5 shows the neutral stability curve as the tangential stress S_t is varied as well as corresponding steady-state solutions. We observe in Figure 5a that specifying $S_t > 0$ is stabilizing as compared to the stress-free boundary conditions ($S_t = 0$). This response can be put in parallel to the pure 1D sheet where it is known that fixing the

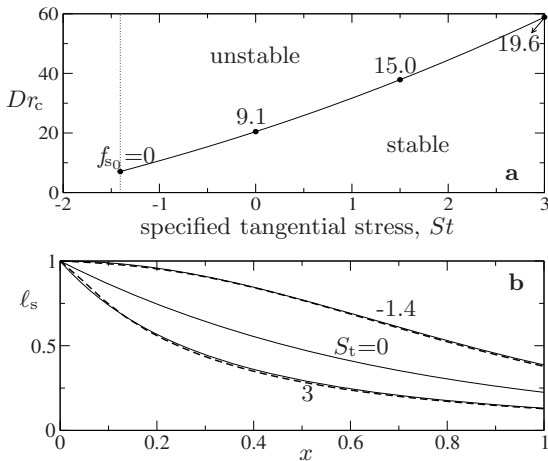


Fig. 5. (a) Neutral stability curve for $a=1/10$ and $S_n=0$, with values of the sheet's tension at the inlet f_{s_0} . (b) Steady-state solutions (solid lines) and 2D COMSOL solutions (dashed lines).

axial tension instead of the take-up speed makes the sheet unconditionally stable [7,13]. But as a consequence of the lateral forcing, the tension in the sheet here depends on the coordinates (in contrast to the stress-free or the pure 1D cases).

We have also indicated in Figure 5a the value of the sheet's tension f_{s_0} at the inlet ($x = 0$) and observe that it increases when S_t is increased. Consequently, the necking phenomenon is reinforced and the final width (at take-up) is further decreased as shown in Figure 5b for $S_t = 3$. On the contrary, $S_t < 0$ acts opposite to the tension induced by the pulling, which has a destabilizing effect and the critical draw ratio is reduced below 20.218. Nevertheless, at $S_t = -1.4$, the tension f_{s_0} at the inlet vanishes, and the neutral stability curve ends as observed in Figure 5a. The corresponding shape of the sheet is therefore the widest that can be obtained with a pure tangential stress specified at the edge boundary, at least if S_t is kept constant. As a consequence, a constant-width sheet is not obtainable by acting exclusively on S_t .

4 Specified transverse velocity

In this section, we model the situation where a time-independent edge velocity is specified, namely $w_\ell = w_\ell(x)$. This type of forcing is motivated by the float glass application as detailed at the end of the section. As a consequence, both S_n and S_t can be different from zero and the shape of the sheet as well as its stability will depend on the distribution of w_ℓ . Rewriting the appropriate form of the momentum equation (15) yields

$$\partial_x \sigma_{xx} = -\sigma_{xx} \frac{\partial_x h}{h} - \frac{1}{a} \partial_x \left(\frac{w_\ell}{\ell} \right). \quad (36)$$

The stress relation (13a) is also rewritten as

$$\partial_x u = \frac{\sigma_{xx}}{4} - \frac{w_\ell}{2a\ell}, \quad (37)$$

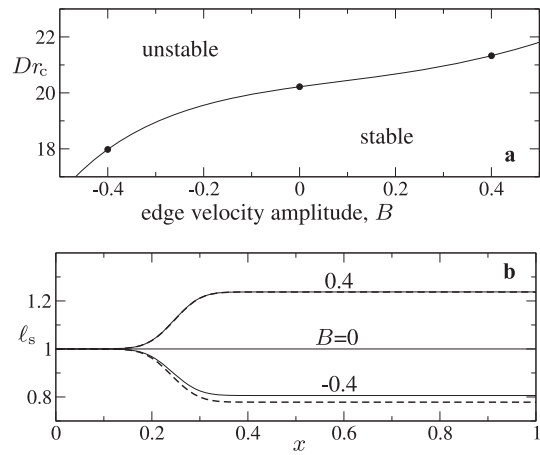


Fig. 6. (a) Neutral stability curve for $a = 1/10$ and a specified edge speed \bar{w}_ℓ with $x' = 1/4$ and $s = 1/8$. (b) Steady-state solutions (solid lines) and 2D COMSOL solutions (dashed lines).

and the system is closed with (12a) and (12b), provided an explicit form of $w_\ell(x)$ is given. Let us assume here a Gaussian function

$$w_\ell = B e^{-\frac{4(x-x')^2}{s^2}}, \quad (38)$$

where B is the amplitude and x' and s are fitting parameters.

Figure 6 shows the corresponding stability map as well as typical shapes of the sheet. For positive speeds ($B > 0$) the system is stabilized while it is destabilized for negative speeds ($B < 0$), as depicted in Figure 6a. In contrast to the case of a pure normal stress (see Sect. 3.2), increasing the width of the sheet by specifying a positive edge velocity (see Fig. 6b for $B = 0.4$) is stabilizing as compared to the constant-width case ($B = 0$). The reason for this response is that here the induced tangential stress component S_t is non-zero and therefore influences the stability of the system. In fact, using (6b) and (13), we can write $S_t = \partial_x w_\ell + w_\ell (\partial_x \ell / \ell) + O(a \partial_x \ell)$, which averaged along the x direction, using (38), gives $\int_0^1 S_t dx \approx 0.05$. Since this average is positive, we expect a stabilizing effect according to results in Section 3.3 for a constant tangential stress specified at the edge. This stabilization due to the tangential component S_t of the induced stress wins, for this specific case, against the destabilization of its normal component S_n .

Note the Gaussian form of the edge speed aims to mimic the effect of a 'edge roll' in the float glass process, i.e. a cogwheel that grips outward the edge of the melted glass sheet (see Introduction). Even though the action of such an 'edge roll' is localized in space, the high viscosity of the melted glass ensures the coherence of the flow such that a Gaussian shape is a fairly good continuous approximation. We note that we have also tried other velocity functions that characterize more precisely practical conditions (not presented here). However, no difference has been found in the general conclusions, which are that, though the stability properties of the system depend

Table 2. Different situations investigated in this work and stability behavior as compared to two reference cases.

Edge boundary conditions	As compared to the 1D case		As compared to the stress-free case	
	Stabilizing	Destabilizing	Stabilizing	Destabilizing
Stress-free	always	never	identity	
Pure normal stress	$S_n < S_n^*$	$S_n > S_n^*$	for $\varepsilon < a \ll 1$, $S_n \ll S_n^*$	for $a \gtrsim 1$, $\forall S_n > 0$
Pure tangential stress	not possible		$S_t > 0$	$S_t < 0$
Specified velocity	$w_\ell > 0$	$w_\ell < 0$	not investigated	

on the prescribed velocity function, they can be rationalized by computing separately the induced stress components S_n and S_t .

5 Concluding remarks

In this paper, we have proposed a framework to investigate the dynamics of a two-dimensional stretching sheet by using a one-dimensional model and considering various lateral boundary conditions. With the model, we have addressed the most generic situations such as the departure from the 1D parallel flow and from the stress-free conditions by applying appropriate boundary conditions.

More specifically, we have derived a one-dimensional model for the thickness h , the width ℓ , the axial velocity u and the axial stress σ_{xx} to describe the behavior of a two-dimensional viscous sheet. We have systematically analyzed the shape and the stability of the sheet with various boundary conditions applied at the edges and thus have explored the role of lateral shaping. The results are summarized in Table 2. We have shown for instance that widening a viscous sheet is destabilizing as compared to a constant-width sheet when a pure normal stress is applied at the edges while it is stabilizing when the edge velocity is specified due to a resulting non-zero tangential component that arises in the latter case. The reality is more complex, since the edge velocity is only specified where the edge rollers are located and stress-free boundary conditions should apply in between each edge roller and after the last edge roller. So more realistic forcing would mean mixed boundary conditions among those proposed in the paper. However, based on our knowledge of such a process, the one-dimensional model presented here allows to satisfactorily assess the shape of the glass sheet.

As for possible extension, it might be of practical interest to compute the speed distribution w_ℓ in the case of the stress-free conditions at the edge corresponding to the axial stress balance $\partial_x(h\ell\sigma_{xx}) = 0$. With the use of (36), the time-dependent edge speed $w_\ell = w_\ell^*$ corresponding to stress-free conditions would then be solution of $\partial_x w_\ell = (w_\ell/\ell + a\sigma_{xx})\partial_x \ell$. Next, as done for the pure normal stress condition (see Sect. 3.2), one could consider $w_\ell = c w_\ell^*$ and probe the parameter c to study the departure from the stress-free conditions when specifying the edge velocity.

The 1D model, at least for small aspect ratios, is found to satisfactorily describe the two-dimensional features of

a stretching sheet (as compared with 2D COMSOL computations). Therefore, due to its simplicity, the 1D model should allow investigation of the shape and the stability of a sheet with a large variety of boundary conditions corresponding to practical applications. Such *lateral shaping* can indeed be a design tool. We have furthermore shown the possibility of controlling the draw resonance with time-dependent lateral stress (Sect. 3.2), which could be of significant practical interest, mostly because the longitudinal control in the pure 1D case is not feasible and produces instead new instabilities at low draw ratios [13].

We thank Saint-Gobain Recherche for support of this investigation and R. Gy for useful discussions.

References

1. L.A.B. Pilkington, Proc. T. Soc. London, Ser. A **314**, 1 (1969)
2. O.S. Narayanaswamy, J. Amer. Ceram. Soc. **60**, 1 (1977)
3. J.R.A. Pearson, *Mechanics of Polymer Processing* (Elsevier Applied Science Publishers, 1985)
4. D. Silagy, Y. Demay, J.-F. Agassant, Polym. Eng. Sci. **36**, 2614 (1996)
5. D. Silagy, Y. Demay, J.-F. Agassant, J. Non-Newtonian Fluid Mech. **79**, 563 (1998)
6. B. Scheid, S. Quiligotti, B. Tran, R. Gy, H. Stone, On the (de)stabilization of draw resonance due to cooling, J. Fluid Mech., Submitted
7. Y.L. Yeow, J. Fluid Mech. **66**, 613 (1974)
8. C. Sollogoub, Y. Demay, J.-F. Agassant, J. Non-Newtonian Fluid Mech. **138**, 76 (2006)
9. C.W. Hirt, A.A. Amsden, J.L. Cook, J. Comp. Phys. **14**, 227 (1974)
10. M.A. Matovich, J.R.A. Pearson, Ind. Eng. Chem. Fundam. **8**, 512 (1969)
11. E.J. Doedel, A. Champneys, T. Fairfrieve, Y. Kuznetsov, B. Sandstede, X. Wang, AUTO97 *continuation and bifurcation software for ordinary differential equations* (Montreal Concordia University, 1997), AUTO software is freely distributed on <http://indy.cs.concordia.ca/auto/>
12. H.B. Keller, Numerical solution of bifurcation and nonlinear eigenvalue problems, *Applications of Bifurcation Theory*, edited by P.H. Rabinowitz, 3rd edn. (Academic Press, New York, 1977), pp. 359–384
13. M. Renardy, SIAM J. Appl. Math. **66**, 1261 (2006)
14. G.I. Taylor, J. Fluid Mech. **10**, 305 (1961)